Earthquakes and Structures, *Vol. 15, No. 2 (2018) 203-214*
DOI: https://doi.org/10.12989/eas.2018.15.2.203

Reinforced concrete core-walls connected by a bridge with buckling restrained braces subjected to seismic loads

Hamid Beiraghi*

Department of Civil Engineering, Mahdishahr Branch, Islamic Azad University, Mahdishahr, Iran

(Received February 20, 2018, Revised May 7, 2018, Accepted May 17, 2018)

Abstract. Deflection control in tall buildings is a challenging issue. Connecting of the towers is an interesting idea for architects as well as structural engineers. In this paper, two reinforced concrete core-wall towers are connected by a truss bridge with buckling restrained braces. The buildings are 40 and 60-story. The effect of the location of the bridge is investigated. Response spectrum analysis of the linear models is used to obtain the design demands and the systems are designed according to the reliable codes. Then, nonlinear time history analysis at maximum considered earthquake is performed to assess the seismic responses of the systems subjected to far-field and near-field record sets. Fiber elements are used for the reinforced concrete walls. On average, the inter-story drift ratio demand will be minimized when the bridge is approximately located at a height equal to 0.825 times the total height of the building. Besides, because of whipping effects, maximum roof acceleration demand is approximately two times the peak ground acceleration. Plasticity extends near the base and also in major areas of the walls subjected to the seismic loads.

Keywords: reinforced concrete core-wall; connected building; buckling restrained braces; truss bridge; time history analysis

1. Introduction

Structures are supposed to experience inelastic deformation during moderate to severe earthquakes. In cantilever slender reinforced concrete (RC) shear walls, the flexural plastic hinge is preferred to occur at the base of the wall. This occurrence leads to the ductile behavior and energy dissipation in the shear wall systems (Paulay *et al*. 1992, Beiraghi 2017a). In some tall buildings, the RC core-wall is the only lateral load bearing system (Saad *et al*. 2016). Displacement control of the tall cantilever core-wall buildings subjected to the seismic loads is very difficult for designers.

Subjected to seismic loads, the conventional steel bracing members undergo large deformations in the post-buckling range (Rai *et al*. 2003). They lose their axial stiffness after buckling under compressive force. In recent years, a new type of bracing named buckling restrained braces (BRBs) has been used in structure industry to overcome some of the shortcomings of conventional braces. In this new type, load displacement characteristic of members is approximately identical in both axial compression and tension (Tremblay *et al*. 2006, Asgarian *et al*. 2008,Guneyisi *et al*. 2014). As shown in future sections, unlike conventional braces, BRBs have the capability to achieve stable hysteretic behavior and significant ductility by withstanding compression yielding before buckling (Black *et al*. 2002). This kind of members can be used in the truss bridge between two towers to dissipate energy.

RC core-wall systems are popular in tall buildings, as they provide a good view and natural light for the user. It seems that the formation of only one plastic hinge at the base of the cantilever walls leads to the concentration of inelastic deformation in a limited area of the wall and therefore increases the damage potential in that area (Beiraghi *et al*. 2016a, 2017b). However, this issue changes in connected core-wall structures. A more spectacular view can be provided by a sky bridge between two towers. (Luong *et al*. 2012). Tall connected structures are relatively new types of structural systems that attracted the attention of designers in recent years (Jiang *et al*. 2004). In some countries like China, the use of high-rise connected buildings is more popular. Connecting two RC core-walls by a truss bridge may prevent them from excessive lateral displacement. However, few tall buildings around the world have used the idea of connected towers and few numerical (Ozuygur 2015, Ozuygur 2016) and experimental studies have been conducted in this regard. At present, the seismic response of such structures has not been sufficiently investigated. Some analytical models of structures connected by damper devices have been investigated by Xu *et al*. (1999), Chen *et al*. (2010) and Richardson *et al*. (2011) to analyze seismic response of the systems. For a single detached building, the mode shapes are affected by a power function, while the mode shapes of connected structures could be affected by the bridge and hence may not follow a power function (Lim 2009, Lim *et al*. 2011).

It is worth noting that the near-field (NF) ground motions causes more significant damage on the structures compared the far-field (FF) motions (Mortezaei and Ronagh 2013). In this article, two reinforced concrete core-wall

*Corresponding author, Ph.D.
E-mail: h.beiraghi@msh-iau.ac.ir

http://www.techno-press.com/journals/eas&subpage=7
ISSN: 2092-7614 (Print), 2092-7622 (Online)

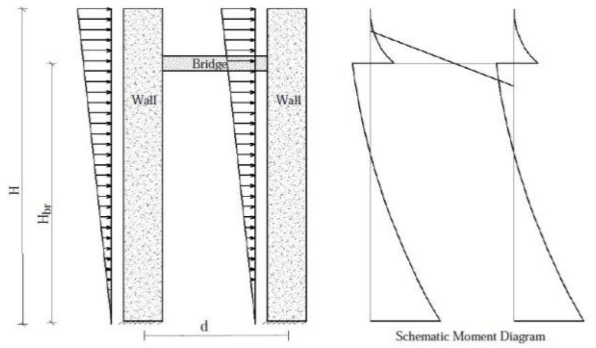

Fig. 1 General concepts of the system and moment diagram subjected to lateral load

towers are connected by a truss bridge with buckling restrained braces. The systems are 40 and 60-story buildings. The effect of the location of the bridge is investigated. Response spectrum analysis of the linear models is used to calculate the design demands and the systems are designed according to the reliable codes. Then, fiber elements are used for reinforced concrete core-walls and nonlinear time history analysis is performed to assess the seismic responses of the systems subjected to FF and NF record sets.

2. Main idea

Connecting two RC core-walls by a bridge changes the moment distribution along each core-wall. Fig. 1 shows the schematic moment diagram in the core-wall and in the bridge, subjected to lateral load. The effect of the truss bridge on the core-wall is similar to that of outrigger truss on the core-wall. When the structure is subjected to lateral load, a negative moment is exerted by the truss bridge on each core. Furthermore, core-wall rotation at the bridge level and also the lateral drift will be reduced.

3. Design procedure

40 and 60-story buildings, the general plan of which are shown in Fig. 2, are considered in this research. The system consists of two RC core-wall connected by a BRB truss bridge. The floors are assumed to be made of post tensioned concrete without beams. There is not any beam in the typical floor of each tower model. In each tower, the gravity load is carried by peripheral columns as well as the core-wall. The peripheral columns do not contribute in lateral load bearing. The contribution of post-tensioned slabs in carrying lateral loads is also negligible (Panagiotou *et al*. 2009). Therefore, the seismic loads are mainly carried by the two core-walls and the bridge action.

3.1 First design approach

Response spectrum analysis (RSA), a procedure which combines the responses of different modes of vibration, is used to calculate the design demands. Design spectrum used in the design procedure is represented in Fig. 3. This spectrum pertains to 5% of damping. Specified compressive strength of concrete, f_c=45 MPa, and specified yield strength of reinforcement bars, f_y=400 MPa, were used.

ASCE-10, AISC-10 and ACI318-14 are applied for the analysis and design of the systems (AISC 2010, ACI 318-11 2011, ASCE/SEI 7-2010 2010). Response modification coefficient is equal to 6. In order to accomplish finite element model, perform linear analysis and design the components, ETABS software was applied. Shell elements were used for wall modeling, and steel BRB elements for horizontal and diagonal truss elements of the bridge. In each tower, a rigid diaphragm was used for the floors. Since the elements of the bridge are supposed to carry the axial loads during earthquakes, the rigid diaphragm was not used for the stories of the bridge between the towers.

As the effect of the bridge on the towers is similar to that of the outrigger arm on the core of an outrigger system, this concept can be useful to determine the level of the bridge. Locating the most effective level for the bridge depends on the relative stiffness of the truss bridge and the core-wall. It is worth noting that the most effective level also depends on the selected response, e.g., the roof drift, the inter-story drift ratio etc. (Beiraghi *et al*. 2016b). Besides, there is not any general recommendation about the optimum location of an outrigger arm in real seismic structural behavior. While many of the previous suggestions are related to elastic models, the structures experience nonlinear behavior in sever earthquakes. For core-wall systems with outriggers, the optimum location of the outrigger has been investigated in linear structures

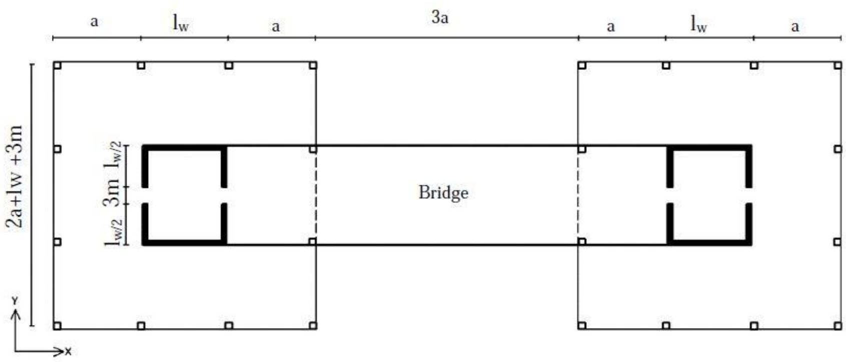

Fig. 2 Plan and dimension of the system

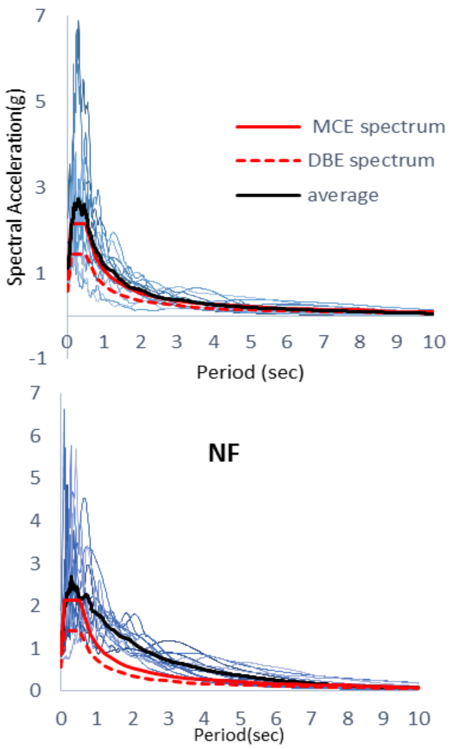

Fig. 3 MCE and DBE level spectra; individual and average spectra of NF and FF records

subjected to lateral loads with a triangular pattern. Assuming a triangular lateral load pattern and a uniform cross-section for the core, outrigger and the columns, a graphical solution has been presented by Smith and Salim (1981). Similar to the effect of the bridge on the core in connected core-walls, the outrigger may exert a moment on the core. Taking this fact into consideration, the bridge may

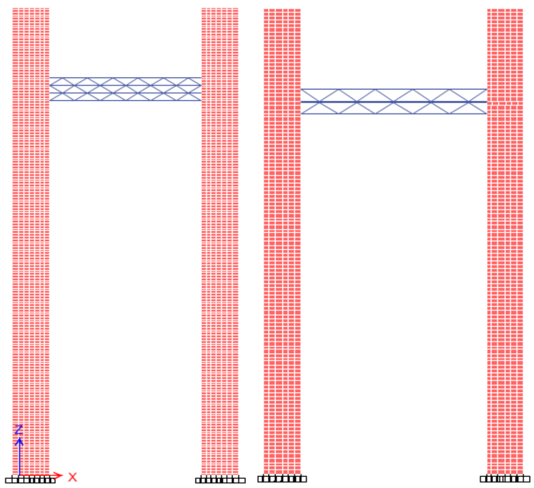

Fig. 4 Elevation of the elastic finite element model used in design process with bridge level at 0.825H. (All elements of the bridge truss are BRBs)

approximately be located at a height equal to 0.7 times the total height of the building. According to Smith and Salim (1981), in case of earthquake loads, this height is higher. In this study, three height levels for the bridge are assumed: at the 0.725H, 0.825H and roof of the 60-story building (H is the total height of the buildings). Denomination is for example as 60St-B@0.825H. The thickness of the wall in three structural models were identical and each of them is designed to find the vertical reinforcement. The elements of the truss bridge are made of buckling restrained braces. In all three structural models, the minimum base shear prescribed by the ASCE-10 controlled the design. Finite element model in the design procedure has been presented in Fig. 4. Lateral load direction is only the *x* direction in

Table 1 Specification of the designed models

	60ST-B@Roof	60ST-B @0.825H	60ST-B @0.725H	60ST-B @0.825H.W	40ST-B @0.825H
Analysis approach	ASCE	ASCE	ASCE	ASCE-w/o applying Min. base shear	ASCE
Level of bridge	roof	0.825H	0.725H	0.825H	0.825H
Lw (m)	15	15	15	15	10
a (m)	12	12	12	12	10
Wall thickness (cm)	90	90	90	55	60
Seismic Weight=*W* (1000 Kgf)	191380	191380	191340	167680	71790
No. of bridge stories	3	3	3	3	2
H (m)	210	210	210	210	140
Base shear from RSA/W	0.030	0.030	0.030	0.026	0.036
Base shear from equivalent lateral force procedure /W	0.062	0.062	0.062	0.030	0.062
*T1** (s)	6.99	6.43	6.11	8.19	4.98
T2 (s)	2.008	1.52	1.56	1.85	1.17
T3 (s)	1.35	1.27	1.28	1.59	0.988
Maximum elastic IDR	0.0039	0.0037	0.0035	0.0026	0.0035
Range of force Demand/Capacity in BRB in elastic model	0.73-0.92	0.7-0.9	0.75-0.93	0.72-0.94	0.7-0.9

Table 2 Vertical reinforcement ratio

60ST-B@Roof		60ST-B @0.825H		60ST-B @0.725H		60ST-B @0.825H.W		40ST-B @0.825H	
Stories	ρ%	Stories	ρ%	Stories	ρ%	Stories	ρ%	Stories	ρ%
1-6	3.65	1-6	3.7	1-6	3.74	1-6	3.4	1-4	3.75
7-12	2.33	7-12	2.37	7-12	2.3	7-12	1.6	5-8	2.44
13-18	1.48	13-18	1.42	13-18	1.32	13-18	0.25	9-12	1.52
19-24	0.97	19-24	0.85	19-24	0.79	19-24	0.25	13-16	0.99
25-30	0.74	25-30	0.67	25-30	0.61	25-30	0.25	17-20	0.77
31-36	0.87	31-36	1.04	31-36	1.12	31-36	0.25	21-24	0.99
37-42	1.21	37-42	1.57	37-42	1.71	37-42	0.64	25-27	1.27
43-48	1.54	43-47	1.94	43-46	1.61	43-47	0.95	28-31	1.59
49-54	1.96	48-51	1.83	47-52	1.06	48-51	0.74	32-33	1.21
55-57	2.08	52-60	0.56	53-60	0.47	52-60	0.25	34-40	0.74
58-60	1.54	-	-	-	-	-	-	-	-

Fig. 2. Table 1 presents main characteristics of the buildings.

3.2 Second design approach

In previously described approach, the minimum design base shear prescribed by ASCE-10 governed the design process. Not to meet this criteria may be regarded as another alternative. Therefore, another structure for the bridge at 0.825H was designed, denominated as 60St-B@0.825HW. In this case, all of the assumptions in the previous section exist, except the fulfillment of the minimum base shear required by ASCE-10.

For all considered systems, there were two criteria in the design procedure: maximum allowable drift ratio and the maximum vertical reinforcement ratio in the wall. In this paper, the maximum allowed vertical reinforcement governing the system was 4% (see Table 2).

4. Modeling in perform-3d

The numerical nonlinear model of the systems was developed in software Perform-3D (Perform-3D 2011). Fiber shear wall element was used to create the RC core-wall. This element utilizes vertical inelastic fibers for the wall panels. The expected concrete and steel bar properties used in the analysis are f_{ce}=58.5 MPa and f_{ye}=460 MPa, respectively (LATBSDC 2014). The schematic view for a fiber shear wall model is presented in Fig. 5. In longitudinal direction, the reinforcement and concrete are simulated as vertical inelastic fibers. The shear force is carried by a horizontal spring. Since the nonlinear shear yielding is not ductile, this kind of failure is unfavorable. Therefore, an elastic behavior is assumed for shear deformation (PERFORM-3D user guide 2006). To model buckling restrained brace members in the truss bridge, BRB element was used. BRB elements solely resist axial forces. A BRB element connects two nodes in the truss bridge. The element consists of an inelastic non-buckling component in series with an elastic bar component. The expected yield strength of the BRB core material is 270 MPa.

Following a proper damping procedure is essential for nonlinear time history analysis (NLTHA). A popular damping procedure to simulate damping phenomena in the analyses of multi-degree-of-freedom buildings is the Rayleigh damping model. This kind of damping is a particular form of viscous damping. In this approach, the damping matrix is mass- and stiffness-proportional. It is believed that Rayleigh damping is not a proper approach for structures because in a real building there is not an appropriate mechanism as assumed in the numerical models. Perform-3D software can also use another approach named modal damping. In order to damp out high-frequency vibrations, the user guide of the software recommends a small amount of Rayleigh damping in addition to modal damping. For using Rayleigh damping, the numbers of two modes are needed. In this research, a modal damping of 2.5% for all modes as well as 0.15% Rayleigh damping for the first and third modes are used as recommended by the software guidelines (PERFORM-3D 2011). When modal damping is selected, a damping matrix in the Perform-3D is made which is based on the mode shapes. The software uses elastic mode shapes and periods

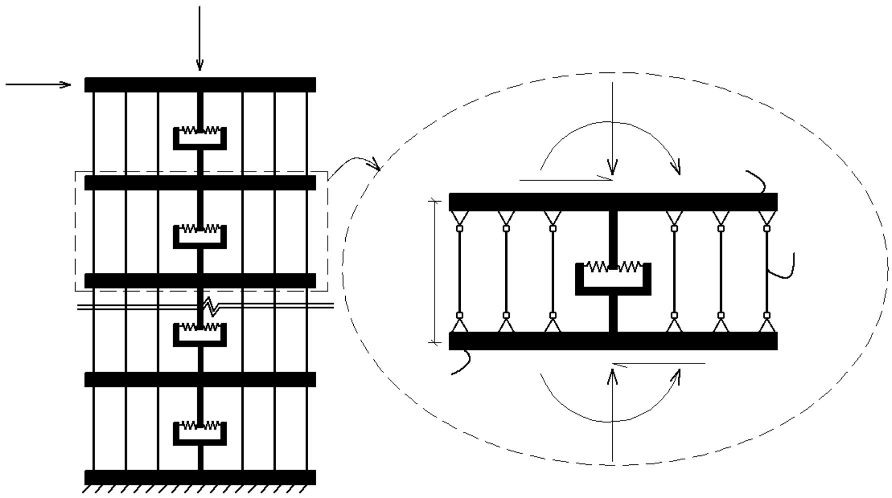

Fig. 5 Schematic of fiber element model for walls

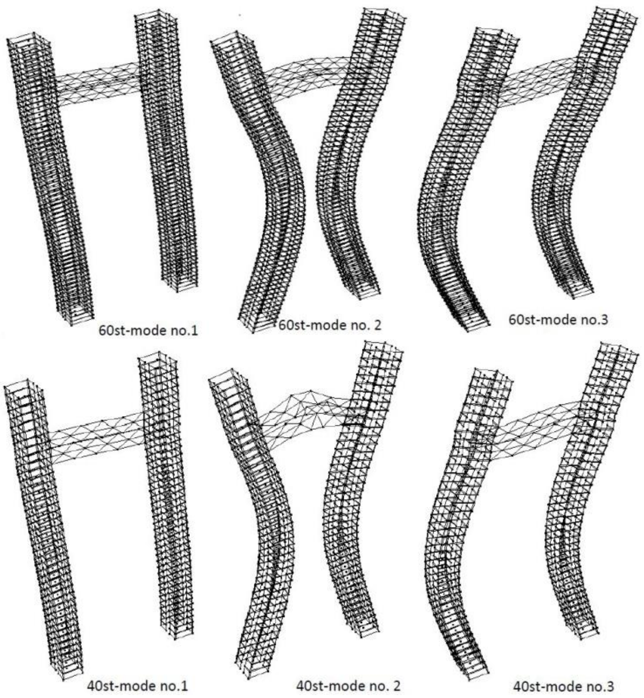

Fig. 6 View of mode shapes of the systems in Perform-3D software (Bridge at 0.825H)

and calculates the damping matrix according to structural dynamics principles (PERFORM-3D user guide, 2006). Nonlinear model in the software with three mode shapes of free vibration along x direction for 40 and 60-story buildings has been presented in Fig. 6.

NLTHA requires use of appropriate ground motions corresponding to maximum considered earthquake (MCE) (LATBSDC 2014). The MCE response spectrum graph level is 1.5 times the design basis earthquake (DBE) response spectrum graph level (ASCE/SEI 7-2010 2010). This study implements the nonlinear analysis for the considered systems subjected to the fault normal component of pulse-like NF and ordinary FF ground motions. For this purpose, a suite of 14 NF and 14 FF ground motions were selected from the record set of FEMA P695 (2009). The specifications of the ground motion are shown in Table 3. The record scaling method is crucial in the NLTHA and can affect the results (Beiraghi *et al*. 2016c, d). The scaling procedure of the records was completed as per ASCE7 (ASCE/SEI 7-2010 2010).

BRB element in Perform-3D is a bar-type element that resists axial force only and has no resistance to torsional or bending forces. This element consists of two bars in series. There is a linear portion incapable of yielding and a

Table 3 List of earthquake records used to carry out nonlinear analysis

	Event name	Year	Station	Record length (s)	PGA*	PGV*	M	Site source distance(km) **
Near-Field record	Imperial valley-06	1979	El centro Array#6	39	0.44	111.9	6.5	27.5
	Imperial valley-06	1979	El centro Array#7	37	0.46	108.9	6.5	27.6
	Irpinia. Italy-01	1980	Sturno	40	0.31	45.5	6.9	30.4
	Superstition-hills-02	1987	Parachute test site	22.3	0.42	106.8	6.5	16
	Loma Prieta	1989	Saratoga-Aloha	40	0.38	55.6	6.9	27.2
	Erizican-Turkey	1992	Erizican	20.8	0.49	95.5	6.7	9
	Cape Mendocino	1992	Petrolia	36	0.63	82.1	7	4.5
	Landers	1992	Lucerne	48	0.79	140.3	7.3	44
	Northridge-01	1994	Rinaldi Receiving Sta	20	0.87	167.3	6.7	10.9
	Northridge-01	1994	Sylmar-Olive View	40	0.73	122.8	6.7	16.8
	Kocaeli/IZT	1999	Izmit	30	0.22	29.8	7.5	5.3
	Chi chi, Taiwan	1999	TCU065	90	0.82	127.7	7.6	26.7
	Chi chi, Taiwan	1999	TCU102	90	0.29	106.6	7.6	45.6
	Duzce	1999	Duzce	26	0.52	79.3	7.1	1.6
Far-Field record	Northridge	1994	Canyon Country-WLC	20	0.48	45	6.7	26.5
	Duzce	1999	Bolu	56	0.82	0.62	7.1	41.3
	Hector Mine	1999	Hector	45.3	0.34	42	7.1	26.5
	Imperial valley	1979	Delta	100	0.35	33	6.5	33.7
	Imperial valley	1979	El centro Array#11	39	0.38	42	6.5	29.4
	Kobe, Japan	1995	Shin- Osaka	41	0.24	38	6.9	46
	Kocaeli, Turkey	1999	Duzce	27.2	0.36	59	7.5	98.2
	Kocaeli, Turkey	1999	Arcelik	30	0.22	40	7.5	53.7
	Landers	1992	Yermo Fire Station	44	0.24	52	7.3	86
	Loma Prieta	1989	Gilroy Array	40	0.56	45	6.9	31.4
	Superstition Hills	1987	El Centro lmp. Co.	40	0.36	46	6.5	35.8
	Superstition Hills	1987	Poe Road (temp)	22.3	0.45	36	6.5	11.2
	Chi chi, Taiwan	1999	Chy101	90	0.44	115	7.6	32
	San Fernando	1971	LA-Hollywood Stor	28	0.21	19	6.6	39.5

* PGA is Peak ground acceleration and PGV is Peak ground velocity; **This is epicentral.

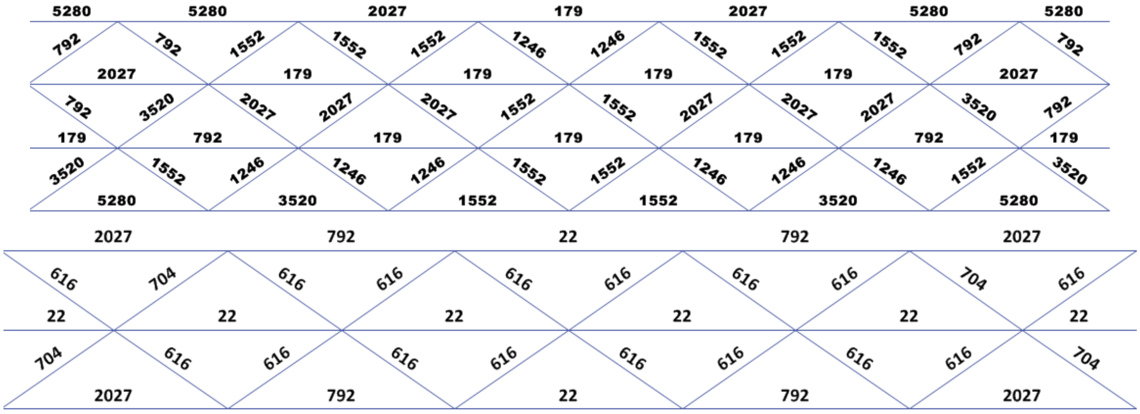

Fig. 7 Core cross section area of the BRBs used in the nonlinear analysis (values are in cm^2)

nonlinear portion capable of yielding. The length of nonlinear portion of a BRB is assumed to be 0.7 of the node-to-node brace element length. The remaining 30% is linear portion that should not yield and this portion consists of the two part that is called transition segment and the end segment. The cross section area of the transition and end segment of BRBs are taken larger than the restrained core cross section. The value of cross section area of transition and end segments (A_t and A_e) were chosen as 1.6 and 2.2 times the cross section area of the core, respectively, and their length were chosen as 0.06 and 0.24 times the total length of the bracing (Nguyen *et al*. 2010). The following equation is used to calculate the cross section area of the yielding core (A_c) of the BRB element for nonlinear modeling (Bosco *et al*. 2013)

$$\frac{L_c}{A_c} = \frac{L_w}{A_{eq}} - \frac{L_e}{A_e} - \frac{L_t}{A_t} \quad (1)$$

Where L_c, L_t, L_e and L_w denominate the lengths of the yielding core, transition segment, end segment and the whole bracing, respectively; Also, A_{eq} is the cross section area of the equivalent brace element obtained from the linear design procedure. Fig. 7 shows core cross section aria of the BRBs used in the nonlinear analysis.

5. Verification of analysis method

Ability of fiber element method to simulate RC shear wall response has been demonstrated by researchers (Orakcal *et al*. 2006). It has been demonstrated that the moment, shear and drift demand distributions from the fiber model of a slender RC wall in Perform-3D were appropriately compatible with the corresponding demand envelopes from the laboratory test wall. More information of the verification is presented in another paper (Beiraghi *et al*. 2015).

To assess the accuracy of BRB elements in the software, an experimental test program accomplished by Merritt *et al*. (2003) was used. As it is obvious from Fig. 8, the hysteretic response has a stable shape and represents a good energy dissipation. Comparing the force-displacement hysteretic responses calculated by numerical model and experimental prototype, illustrates a good similarity.

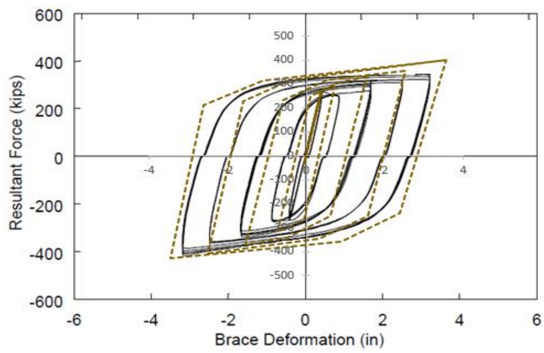

Fig. 8 Comparison of the hysteretic response pertaining to the BRB from numerical (dashed lines) and experimental work of Merritt *et al.* (2003)

6. Responses from analysis

Lateral inter-story drift ratio (IDR) can affect both the lateral resisting structural elements and non-structural components. Design provisions prescribe requirements to achieve a proper structure that can sustain inelastic deformations in the components as well as inter-story drifts. Maximum IDR is a popular index that must be controlled during earthquakes. It is selected here as a criterion to interpret the behavior of the systems. As it is shown in Fig. 9, the mean IDR envelope pertaining to the 60St-B@0.825H has the least maximum IDR. In this case, the maximum value is approximately 0.02, which is considerably smaller than the allowable 3% limit recommended by LATBCD (LATBCD 2014). The reason is that the minimum base shear prescribed by ASCE-10 controlled the design process in the first design approach.

Except the case of 60St-B@Roof, there are two segments in other graphs: one curve below the bridge level and the other above the bridge level. It is desirable to minimize the difference between the two maximum IDRs obtained by two segments. This issue happens in the 60St-B@0.825H Model. As mentioned above, in the second design approach, a new model denominated as 60St-B@0.825HW was created. According to the Fig. 10, it is obvious that in this model the maximum mean IDR is 0.032, which is more than 1.5 times the corresponding values from 60St-B@0.825H and also larger than the

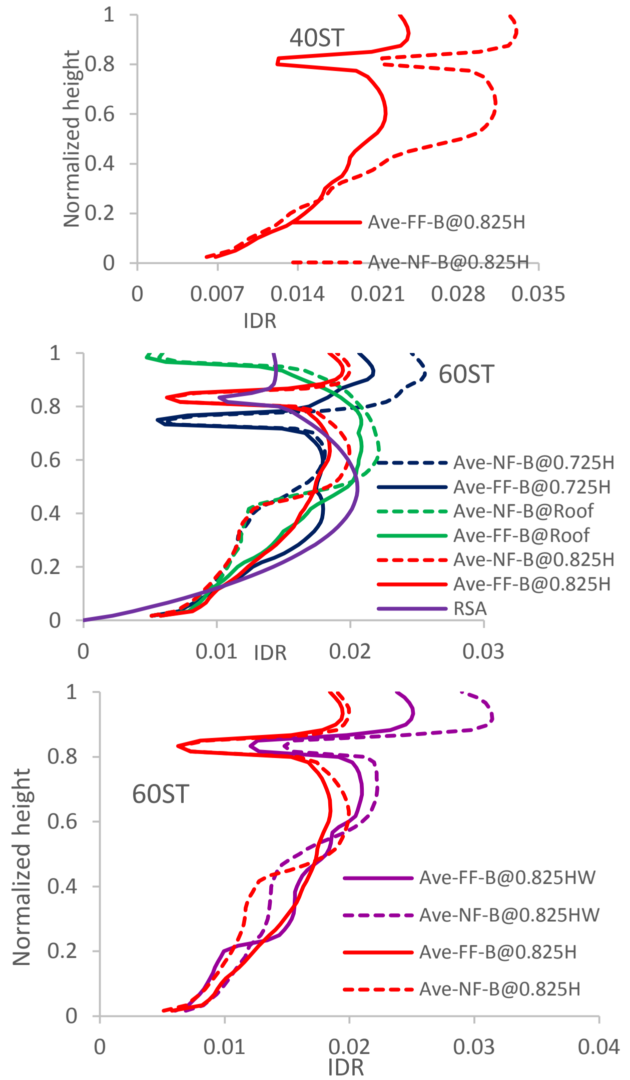

Fig. 10 Comparison between IDR demand envelope for models that fulfill minimum base shear and that do not fulfill that criteria

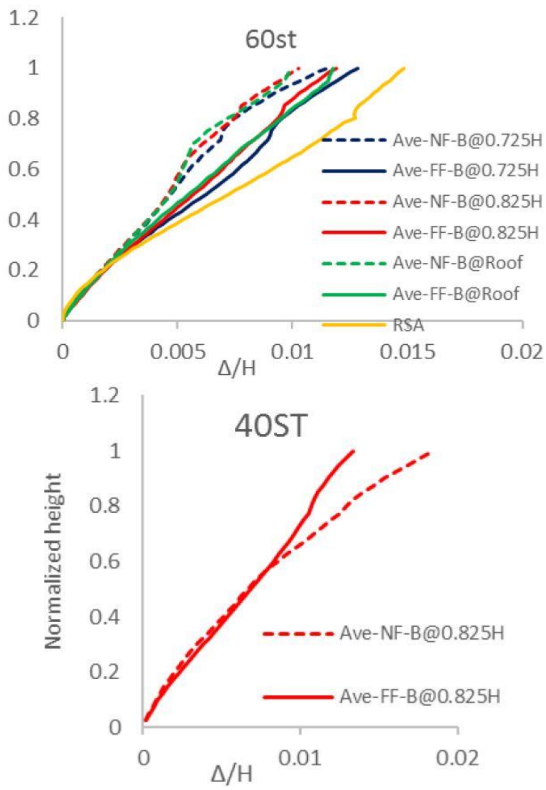

Fig. 11 Average lateral displacement demand envelope along the height of the models subjected to NF and FF events

recommended 0.03 limitation. As other responses were not also reasonable, this approach is neither recommended nor investigated anymore.

For 60-story buildings, Fig. 9 generally demonstrates that, in comparison with the FF records, the NF records cause a larger maximum IDR. If the bridge is located at 0.725H, the maximum IDR from NF records is approximately 1.2 times the corresponding value calculated from FF records. Besides, in this case, **t**he difference between the upper segment and the lower one is rather large. If the bridge is located at the roof level, the form of the mean maximum IDR curve will be different. There is only one peak around the mid-height. The maximum IDR is smaller than the results of the case of 0.725H. But, this value is larger than the corresponding value obtained from the case of 0.825H. If the bridge is located at 0.825H, there is a balance between the upper and the lower curves. Also, the IDR obtained from linear RSA has been amplified by deflection amplification factor and plotted for the 60St-B@0.825H. Deflection amplification factor equal to 5.5 is used to estimate a realistic lateral drift under a seismic load at DBE level (ASCE/SEI 7-2010 2010). It is obvious that value of this curve is relatively small at the region above the bridge level. This happens because in nonlinear cases, plasticity extends in the wall just adjacent above the bridge level. This phenomenon is related to whipping effects. Using the DBE level in the linear analysis is another reason.

For 40-story buildings, the mean IDR envelope of 40St-B@0.825H has been plotted in Fig. 9. In this case, the maximum IDR from NF records is approximately 1.4 times the corresponding value calculated from FF records. Because the 0.825H was selected as a desirable location for the bridge, other levels were not examined for 40-story buildings.

Fig. 11 indicates the lateral displacement of the systems along the height. Horizontal axis is normalized by dividing by the total height. On average, for the 60-story buildings, roof displacement obtained from FF records is approximately 1.15 times the corresponding value from NF records, while this coefficient for the 40-story building is 1.35. Displacement from linear RSA is also plotted for 60St-B@0.825H. Roof displacement from this approach is magnified by a displacement magnification factor, C_d, equal to 5.5, as recommended by ASCE. The results show that the roof displacement in this approach is approximately 1.35 times the mean value from all NLTHA by using NF and FF records. The reason is that in the NLTHA, the direction of roof movement may be opposite to that of the lower part movement. But, to obtain the maximum response, the RSA procedure uses square root of the sum of the squares

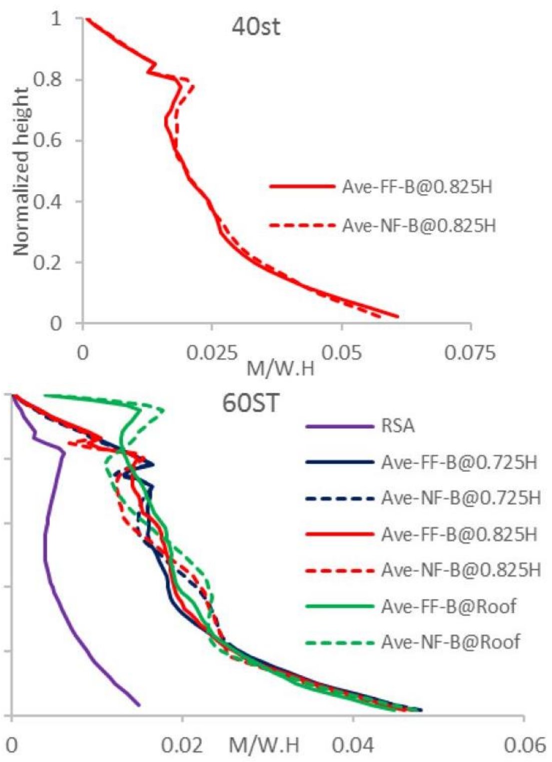

Fig. 12 Average moment demand envelope along the height of one core subjected to NF and FF events

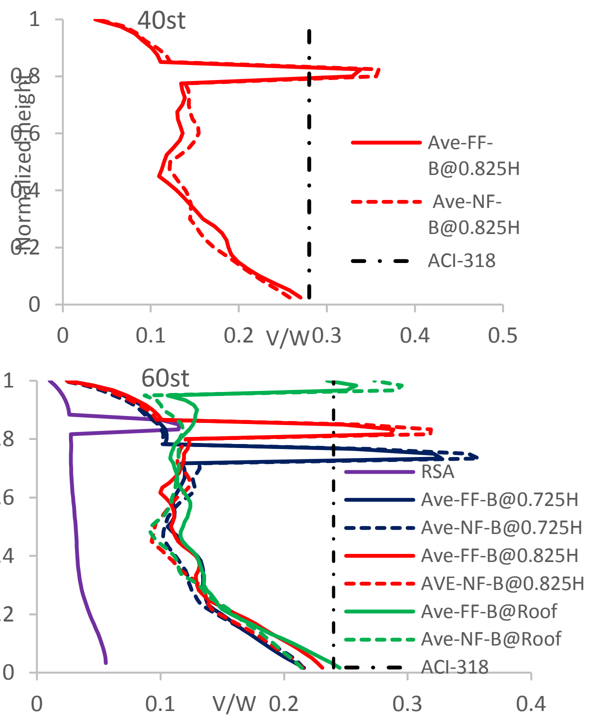

Fig. 13 Average shear demand envelope along the height of one core subjected to NF and FF events

method.

Mean moment demand envelope along the height of one core-wall of the systems has been plotted in Fig. 12. As the plasticity extends approximately all over the core-wall, the moment demand from NF and FF record sets have an insignificant difference. For all cases, especially at the lower half of the buildings, the moment demands are approximately identical for them. Just below the bridge level, there is an increase in the moment diagram since the bridge exerts a flexural moment on the core-wall. For bridge at 0.825H, the general trend of the mean moment demand envelope obtained from NLTHA is similar to the corresponding graph of the linear RSA, but its value is much larger. Some of the reasons include: using expected values for the material strength of NLTHA, using MCE level for NLTHA, difference between the target spectrum and the mean spectrum of the earthquakes, the effect of overstrength of material, the effect of expected strength and the effect of load combination.

Fig. 13 shows the mean shear demand envelope along the height of one core-wall. Similar to the moment diagram, in each structure, the shear demand from NF and FF records is identical. Besides, for 60-story systems, except for the bridge level, the general shear demand from different buildings is approximately similar. Because of bridge action, there is a sudden increase in the shear demand of the core-wall at the bridge level. It is worth noting that according to the ACI318, the maximum allowable shear demand in one core-wall is $2/3Acvfce^{0.5}$, where A_{cv} is the web cross-section area of the core-wall. This value has been plotted in Fig. 13. In some areas near the bridge, it is obvious that the shear demand from NLTHA exceeds this limitation. It is better to increase the wall thickness in the systems.

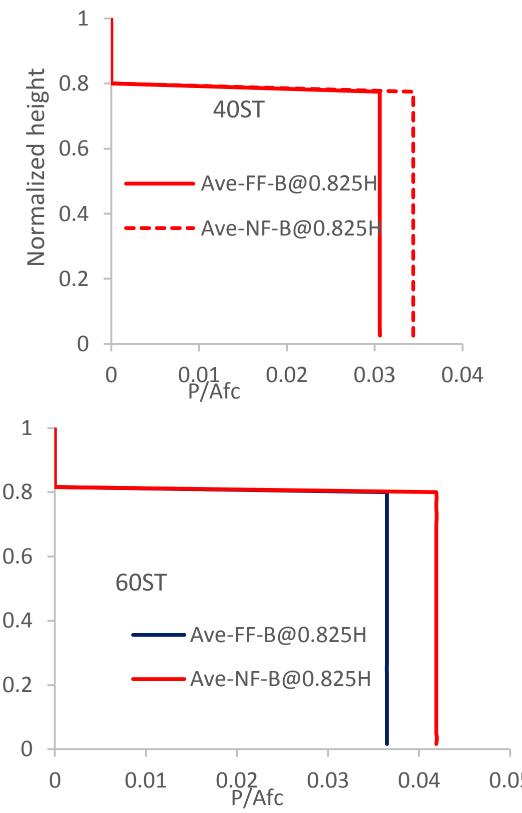

Fig. 14 Average normalized axial force demand envelope along the height of one core subjected to NF and FF events (the gravity load effect is not included)

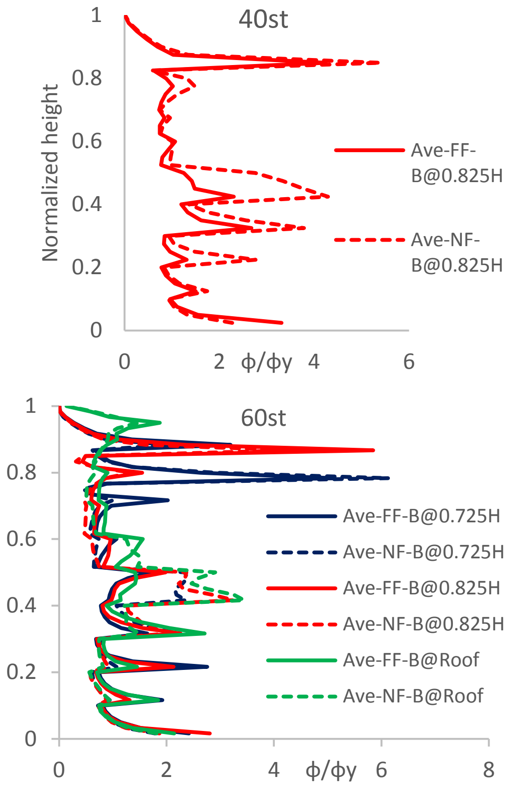

Fig. 15 Average curvature ductility demand envelope along the height of one core subjected to NF and FF events

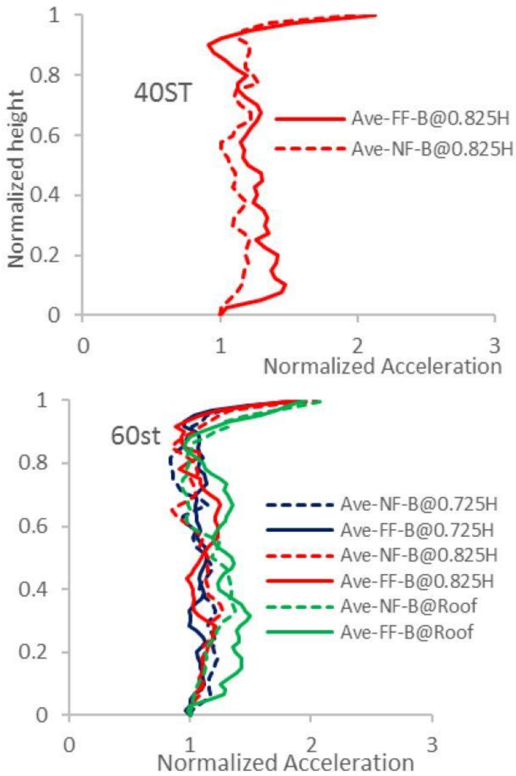

Fig. 16 Average horizontal acceleration demand envelope along height subjected to NF and FF events (the ground level value is normalized to unit)

Because of the bridge action, earthquake loads lead to axial forces in the core-wall. The normalized mean axial force demand solely from earthquake loads has been shown in Fig. 14. The axial force of one core-wall is divided by the product of the cross-section area and concrete strength of the core-wall (*P/Ag.fc*). This ratio is constant in the level below the bridge, and for 60-story buildings subjected to the FF records, for example, is equal to 0.036. The action of the bridge between the two towers is like the action of the coupling beam in coupled RC walls. The coupling ratio (CR) can be calculated by the following equation

$$CR = \frac{F.d}{F.d+2M} \tag{2}$$

Where F is the maximum axial force in the core-wall, M is the maximum moment at the base of one core-wall and d is the horizontal center to center distance between the core-walls. On average, this value is approximately 27% for the considered models.

Curvature ductility demand in the core-wall is a good measurement of the plasticity extension in the core-wall. Curvature ductility is defined as follows

$$Cuvature\ ductility = \frac{\varphi}{\varphi y} \tag{3}$$

Where φy is the yielding curvature obtained from section analysis and φ is the measured curvature demand from NLTHA. One gage per story in the wall has been used to measure the curvature demand. Fig. 15 shows the mean curvature demand envelope in the core-walls. It is obvious that the plasticity extends in major areas of the walls. The local increase in the curves is because of the rebar curtailment. There is a relatively significant increase just above the bridge level which has the maximum value. For example, for the case of 60St-B@0.825H, the maximum curvature ductility demand is approximately 6, and in other locations, the curvature ductility demand is less than 3.5. These are seemingly reasonable values, and the ductility can be provided by confining the concrete using stirrups. For 60-story buildings, the case with least maximum curvature ductility pertaining to the 60St-B@Roof and its value is 3.5.

Floor acceleration demand is an important response to estimate in-plane forces for the design of diaphragms as well as their connections to the lateral load resisting systems. Also, Horizontal accelerations are used to obtain forces for designing non-structural elements and equipment. Fig. 15 shows the mean floor acceleration envelope obtained from structures subjected to the NF and FF earthquakes. On average, maximum floor accelerations are larger than the peak ground acceleration. Furthermore, in all cases, the maximum roof acceleration is approximately two times the peak ground acceleration that is because of the whipping effect. For 60-story buildings, for each NF and FF record sets, the maximum roof acceleration for all three levels of bridge location is identical.

Generally, the maximum strain in the BRB core must be controlled. For 60St-B@0.825H, Fig. 17 plots the normalized strain in the BRB core for the three rows of the diagonal BRBs and four rows of the horizontal BRBs that has been used in the bridge. Fig. 18 plots corresponding

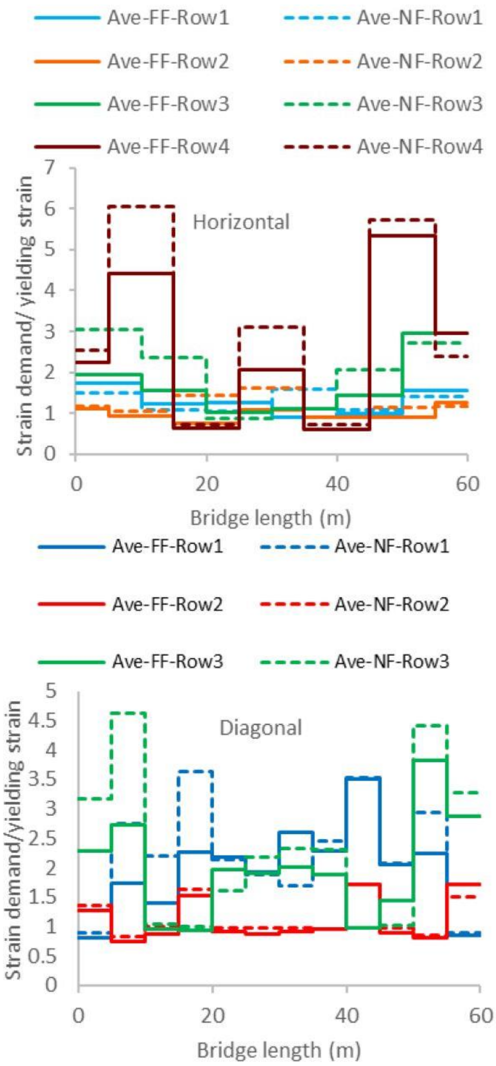

Fig. 17 Average axial strain demand envelope in the horizontal and diagonal BRBs of 60St-B@0.825H along the bridge subjected to NF and FF events

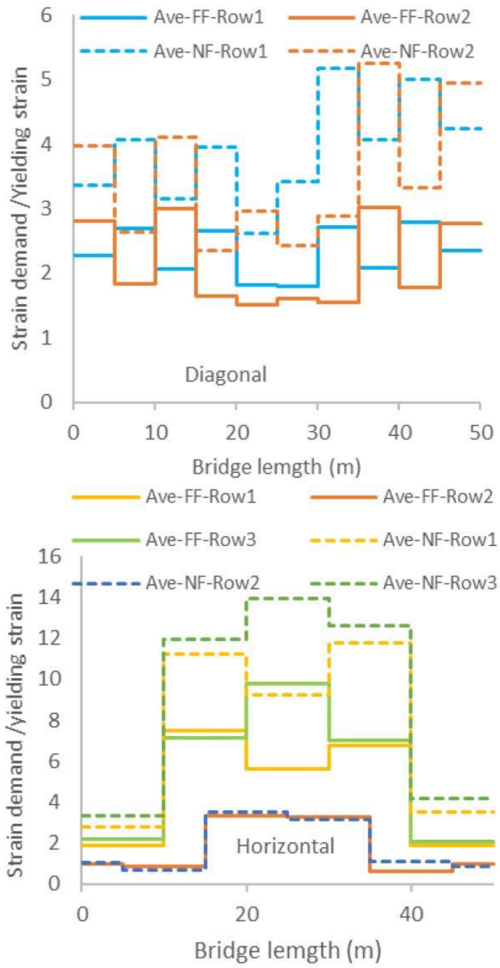

Fig. 18 Average axial strain demand envelope in the horizontal and diagonal BRBs of 40St-B@0.825H along the bridge subjected to NF and FF events

values for the 40-story building. The horizontal axis is the length of the bridge and the vertical axis is the normalized mean maximum axial strain of the core material (axial ductility). To normalize the strain demand, the measured strain demand has been divided by the expected yielding strain equal to 0.00135. It is obvious that for 60-story system the axial ductility in each BRB core subjected to the FF and NF earthquake is almost less than 6 and 4, respectively. In 40-story system, the corresponding values is almost less than maximum allowable value determined in ASCE/SEI 41-13 (2014).

8. Conclusions

In this paper, two reinforced concrete core-wall towers were connected by a truss bridge with buckling restrained braces. The examined systems were 40 and 60-story buildings. Response spectrum analysis of the linear models was used to design the systems according to the prescriptive codes. Nonlinear time history analysis was then performed to assess the seismic responses of the systems subjected to far-field and near-field record sets at maximum considered earthquake level. Fiber elements were used for the reinforced concrete walls. The general responses of the systems subjected to the earthquake records like inter-story drift and strains were in the acceptable range and it seems that this system is effective for tall buildings. For the considered systems, the following results can be concluded:

- If the minimum base shear prescribed by codes was not fulfilled in the design procedure, the maximum inter-story drift ratio in the nonlinear time history analysis would exceed the allowable values.
- For the mean maximum inter-story drift ratio envelope, except for the case of bridge located at the roof, there are two segments in the graphs: one segment is below the bridge level and the other is above it. It is desirable to minimize the difference between the two maximum inter-story drift ratios in two segments. This happens when the bridge is located at 0.825H. In this case, the maximum IDR is approximately 0.02, which is smaller than the allowable 3% limit. Besides, the inter-story drift ratio graph calculated from linear RSA underestimated the real values obtained from nonlinear time history analysis at the region above the bridge

level. This happens because in nonlinear cases, significant plasticity extends above the bridge level in the wall. This phenomenon is related to whipping effects.

• The general trend of the mean moment demand envelope obtained from NLTHA is similar to corresponding graph from the linear RSA, but the values from NLTHA are much larger. Some of the reasons are: using expected values for the material strength in NLTHA, using MCE level in NLTHA, difference between the target spectrum and mean spectrum of the record sets, the effect of system and material overstrength.

• The maximum shear demand obtained from NLTHA exceeds the code prescriptive values in some areas near the bridge.

• On average, the coupling ratio between two towers connected by the truss bridge is approximately 27% for the considered models.

• Plasticity extends near the base and also in major areas of the walls subjected to the seismic loads. Curvature ductility demand increases significantly just above the bridge level which has the maximum value along the structure height. For example, for the case of 60St-B@0.825H, the maximum curvature ductility demand just above the bridge is approximately 6, and in other locations along the height, the curvature ductility demand is less than 3.5.

• Generally, when subjected to the earthquakes, maximum floor horizontal accelerations are larger than the peak ground acceleration. Furthermore, in all cases, the maximum roof acceleration is approximately two times the peak ground acceleration caused by the whipping effect.

• The mean maximum strain in each BRB core subjected to FF and NF earthquake is almost less than the maximum allowable value.

• For 40St-B@0.825H system, the mean maximum IDR from NF records is approximately 1.4 times the corresponding value calculated from FF records and this ratio is reduced for 60St-B@0.825H system.

References

ACI 318-11 (2011), Building Code Requirements for Structural Concrete and Commentary, ACI Committee 318, Farmington Hills.

AISC (2010), Seismic Provision for Structural Steel Buildings, American Institute of Steel Construction: Chicago.

Applied Technology Council (2010), ATC-72: Modeling and Acceptance Criteria for Seismic Design and Analysis of Tall Buildings, ATC, Redwood City, CA.

ASCE/SEI 41-13 (2014), Seismic Evaluation and Retrofi t of Existing Buildings. American Society of Civil Engineers, Reston, VA.

ASCE/SEI 7-2010 (2010), Minimum Design Loads for Buildings and Other Structures, American Society of Civil Engineers, Reston, VA.

Asgarian, B. and Amirhesari, N. (2008), "A comparison of dynamic nonlinear behavior of ordinary and buckling restrained braced frames subjected to strong ground motion", *Struct. Des. Tall Spec. Build.*, **17**, 367-86.

Beiraghi, H. (2016), "Fundamental period of masonry infilled moment-resisting steel frame buildings", *Struct. Des. Tall Spec. Build.*, **26**(5), e1342.

Beiraghi, H. (2017a), "Earthquake effects on the energy demand of tall reinforced concrete walls with buckling-restrained brace outriggers", *Struct. Eng. Mech.*, **63**(4), 521-536.

Beiraghi, H. (2017b), "Forward directivity near-fault and far-fault ground motion effects on the responses of tall reinforced concrete walls with buckling-restrained brace outriggers", *Scientia Iranica*, **25**(11), 519-539.

Beiraghi, H. and Siahpolo, N. (2016b), "Seismic assessment of RC core-wall building capable of three plastic hinges with outrigger", *Struct. Des. Tall Spec. Build.*, **26**(2), e1306.

Beiraghi, H., Kheyroddin, A. and Kafi, M.A. (2015), "Nonlinear fiber element analysis of a reinforced concrete shear wall subjected to earthquake records", *Tran. Civil Eng.*, **39**(C2+), 409-422.

Beiraghi, H., Kheyroddin, A. and Kafi, M.A. (2016a), "Forward directivity near-fault and far-fault ground motion effects on the behavior of reinforced concrete wall tall buildings with one and more plastic hinges", *Struct. Des. Tall Spec. Build.,* **25**(11), 519-539.

Beiraghi, H., Kheyroddin, A. and Kafi, M.A. (2016c), "Effect of record scaling on the behavior of reinforced concrete core-wall buildings subjected to near-fault and far-fault earthquakes", *Scientia Iranica*, **24**(3), 884.

Beiraghi, H., Kheyroddin, A. and Kafi, M.A. (2016d), "Energy dissipation of tall core-wall structures with multi-plastic hinges subjected to forward directivity near-fault and far-fault earthquakes", *Struct. Des. Tall Spec. Build.*, **25**(15), 801-820.

Black, C., Makris, N. and Aiken, I. (2002), "Component testing, stability analysis and characterization of buckling-restrained braces", Report No. PEER-2002/08, Pacific Earthquake Engineering Research Center, University of California, Berkeley, CA, USA.

Bosco, M. and Marino, E.M. (2013), "Design method and behavior factor for steel frames with buckling restrained braces", *Earthq. Eng. Struct. Dyn.*, **42**, 1243-1263.

Chen, X. and Han, X. (2010), "Research summary on long-span connected tall building structure with viscous dampers", *Struct. Des. Tall Spec. Build.*, **19**, 439-456.

FEMA P695 (2009), Quantification of Building Seismic Performance Factors (ATC-63 Project), Federal Emergency Management Agency, Washington D.C.

Gerami, M. and Siahpolo, N. (2016), "Proposition of a new method for quick assessment of maximum beam ductility in steel moment frame under higher mode effects", *Scientia Iranica A*, **23**(3), 769-787.

Guneyisi, E.M. and Ameen, N. (2014), "Structural behavior of conventional and buckling restrained braced frames subjected to near-field ground motions", *Earthq. Struct.*, **7**(4), 553-570.

Jiang, J.J., Lu, X.Z. and Ye, L.P. (2004), *Finite Element Analysis of Concrete Structures*, Tsinghua University Press.

LATBSDC (2014), An Alternative Procedure For Seismic Analysis and Design of Tall Buildings Located in the Los Angeles Region, Los Angeles Tall Buildings Structural Design Council, Los Angeles.

Lim, J. (2009), "Structural coupling and wind-induced response of twin tall buildings with a skybridge", Colorado State University.

Lim, J., Bienkiewicz, B. and Richards, E. (2011), "Modeling of structural coupling for assessment of modal properties of twin tall buildings with a skybridge", *J. Wind Eng. Indus. Aerodyn.*, **99**(5), 615-623.

Luong, A. and Kwok, M. (2012), "Finding structural solutions by connecting towers", *CTBUH J.*, 26-31..

Merritt, S., Uang, C.M. and Benzoni, G. (2003), "Subassemblage testing of star seismic buckling restrained braces", TR-2003/04, La Jolla (CA), Univ. of California at San Diego.

Mortezaei, A. and Ronagh, H.R. (2013), "Plastic hinge length of reinforced concrete columns subjected to both far-fault and near-fault ground motions having forward directivity", *Struct. Des. Tall Spec. Build.*, **22**(12), 903-926.

Nguyen, A.H., Chintanapakdee, C. and Hayashikawa, T. (2010), "Assessment of current nonlinear static procedures for seismic evaluation of BRBF buildings", *J. Constr. Steel Res.*, **66**(8-9), 1118-1127.

Ö zuygur, A.R. (2015), "Performance-based seismic design of an irregular tall building in Istanbul-a case study", *Struct.*, **5**, 112-122.

Ö zuygur, A.R. (2015), "Performance-based seismic design of an irregular tall building in Istanbul", *Struct. Des. Tall Spec. Build.*, **24**(10), 703-723.

Panagiotou, M. and Restrepo, J. (2009), "Dual-plastic hinge design concept for reducing higher-mode effects on high-rise cantilever wall buildings", *Earthq. Eng. Struct. Dyn.*, **38**, 1359-1380.

Paulay, T. and Priestley, M. (1992), *Seismic Design of Reinforced Concrete and Masonry Buildings*, Wiley, New York.

PERFORM-3D (2006), Nonlinear Analysis and Performance Assessment for 3D Structures, V.4, User Guide, Computers and Structures, Inc., Berkeley, CA.

PERFORM-3D (2011), Nonlinear Analysis and Performance Assessment for 3D Structures, V.4.0.3, Computers and Structures, Inc., Berkeley, CA.

Rai, D.C. and Goel, S.C. (2003), "Seismic evaluation and upgrading of chevron braced frames", *J. Constr. Steel Res.*, **59**, 971-994.

Richardson, A., Walsh, K.K. and Abdullah, M.M. (2013), "Closed-form equations for coupling linear structures using stiffness and damping elements", *Struct. Control Hlth. Monit.*, **20**(3), 259-281.

Saad, G., Najjar, S.S. and Saddik, F. (2016), "Seismic performance of reinforced concrete shear wall buildings with underground stories", *Earthq. Struct.*, **10**(4), 965-988.

Smith, B.S. and Salim, I. (1981), "Parameter study of outrigger-braced tall building structures", *J. Struct. Div.*, **107**(10), 2001-2014.

Tremblay, R., Bolduc, P., Neville, R. and DeVall, R. (2006), "Seismic testing and performance of buckling restrained bracing systems", *Can. J. Civil Eng.*, **33**, 183-198.

Xu, Y.L., He, Q. and Ko, J.M. (1999), "Dynamic response of damper-connected adjacent buildings under earthquake excitation", *Eng. Struct.*, **21**(2), 135-148.

CC